Macromolecules

Article

pubs.acs.org/Macromolecules

Well-Defined Biomimicking Brush-Polymer Self-Assemblies Revealing Cholesterol- and Phosphorylcholine-Enriched Surface

Changsub Kim,[†] Kyungho Kwon,[†] Jongchan Lee,[†] Heesoo Kim,*[,‡] Keun-Hwa Chae,[§] and Moonhor Ree*[,†]

[†]Division of Advanced Materials Science, Department of Chemistry, Pohang Accelerator Laboratory, and Polymer Research Institute, Pohang University of Science and Technology, Pohang 37673, Republic of Korea

[‡]Department of Microbiology and Dongguk Medical Institute, Dongguk University College of Medicine, Gyeongju 38066, Republic of Korea

[§]Advanced Analysis Centre, Korea Institute of Science and Technology, Seoul 02792, Republic of Korea

S *Supporting Information*

ABSTRACT: We have newly synthesized a series of well-defined brush polyethers bearing cholesterol (Chol) and phosphorylcholine (PC) moieties in various compositions which can mimic cell membrane. They were thermally stable up to at least 230 °C and soluble in common solvents, showing good solution processability. Excitingly, they all favorably self-assembled, forming multibilayer structures with 2_1 chain conformation; in comparison, the brush polyether bearing only PC-bristles formed orthorhombically packed cylinder (OPC) structure with 12_5 helical chain conformation. Such multibilayer structure formations could be driven by a strong self-assembling ability of the Chol-bristle in extended conformation; the multibilayer structure formation was further promoted by the presence of PC-bristles. The OPC structure formation could be driven by a lateral packing ability of the brush polymer chain in the helical confirmation resulted from the minimization of repulsive interactions in the neighbored zwitterionic PC-bristles. Because of such the self-assembling natures, all brush polymers always revealed Chol- and PC-enriched surface. Overall, all brush polyethers of this study successfully mimicked cell membrane features (Chol- and PC-surface based on self-assembling). They are very suitable for uses in the fields required cell membrane surface characteristics.

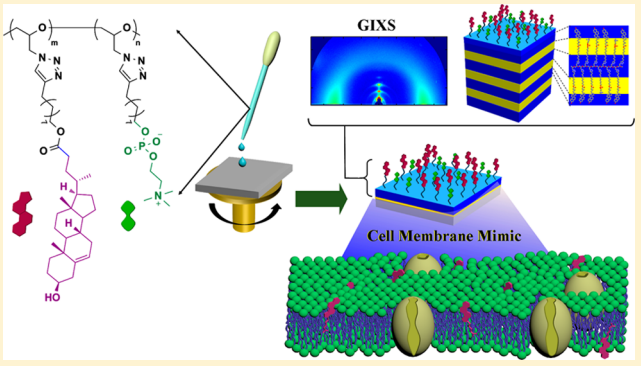

INTRODUCTION

The cell membrane, which is known as plasma membrane or cytoplasmic membrane, is a layer around the cells of all living things.[1,2] Its first important role is to separate the inside of cells from the outside environment, protecting the cells. Its second role is to selectively permit ions and organic molecules and control the movement of substances in and out of cells. The cell membrane is further involved in a variety of cellular processes such as cell adhesion, ion conductivity, and cell signaling and serves as the attachment surface for several extracellular structures.[1,2]

In general, the cell membrane is known to consist of lipids (phospholipid and glycolipid), cholesterols, proteins, and carbohydrates (predominantly glycoproteins).[1,2] In particular, lipids are the major component to build cell membrane as a bilayer. The lipid bilayer primarily serves as a containment unit of living cells. In most cell membranes, lipids are present in approximately 50% of the total mass. The lipid bilayer also forms a matrix in which membrane proteins reside. In addition to such the structural roles, lipids function as regulatory agents in cell growth and adhesion and further participate in the biosynthesis of other biomolecules. Furthermore, they can increase activities of enzymes.[1,2] Cholesterol is also necessary to build and maintain the integrity and mechanical stability of cell membranes.[1−4] It is present in a wide range over a few to 50%, depending on the cells. Cholesterol is known to regulate membrane permeability and fluidity over a wide range of temperatures and anchor molecules, like proteins, in the membrane.[1−4]

In this study, we have aimed to mimic cell membrane in the molecular design and synthesis of new functional high performance polymers. In particular, we have tried to mimic three unique features, namely (i) phospholipid, (ii) cholesterol, and (iii) self-assembling ability, of cell membrane into the development of a novel nanostructured polymer system which can always provide cholesterol (Chol) and phosphorylcholine (PC) enriched surface. A series of poly(oxy(4-(13-cholenoate-nonyl)-1,2,3-trizoyl-1-methyl)ethylene-*ran*-oxy(4-(13-

Received: April 23, 2017
Revised: August 15, 2017
Published: August 28, 2017

DOI: 10.1021/acs.macromol.7b00805
Macromolecules 2017, 50, 6489−6500

Scheme 1. Synthetic Route of PGA-Chol$_m$PC$_n$ Polymers (m = 0−100 mol % Chol-Bristle; n = 100−0 mol % PC-Bristle)

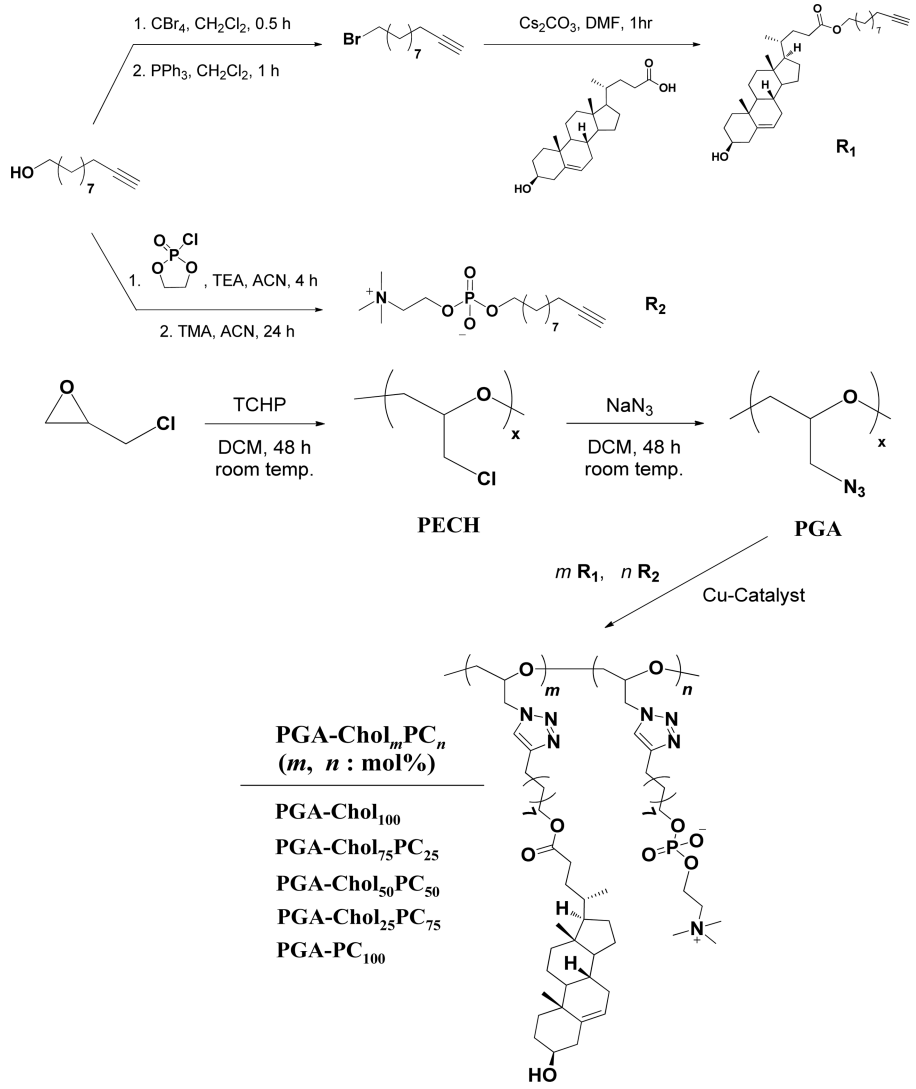

phosphorylcholinenonyl)-1,2,3-trizoyl-1-methyl)ethylene)s (PGA-Chol$_m$PC$_n$: m = 0−100 mol % Chol-containing bristle; n = 100−0 mol % PC-containing bristle) in various compositions were designed and successfully synthesized as a self-assembling brush polymer system bearing Chol- and PC-moieties (Scheme 1). The obtained polymers were stable up to 230 °C or higher temperatures depending on the compositions. They were soluble in various organic solvents including chloroform ($CHCl_3$) and methanol (MeOH). They were investigated in detail by synchrotron grazing incidence X-ray scattering (GIXS) analysis in the aspect of thin film morphology. They all nicely demonstrated self-assembling behaviors, forming multibilayer structure with extended chain conformation or orthorhombic cylinder structure with helical chain conformation depending on the compositions. Based on such self-assembled structures, they always exhibited Chol- and PC-enriched surface. Overall, these polymers successfully mimicked cell membrane features. Therefore, they are potential candidate materials for applications in the fields required cell membrane surface characteristics.

EXPERIMENTAL SECTION

Synthesis. All materials were purchased from Sigma-Aldrich (St. Louis, MO) and Tokyo Chemical Industry (TCI, Tokyo, Japan) and used as received unless otherwise noted. 1-Cholenylundec-10-yne (**R1**, Scheme 1) as ethyne-functionalized Chol-bristle was synthesized in a two-step reaction by using the synthetic information in the literature.[5−7] In the first step, 10-undecyn-1-ol (1 g, 5.94 mmol) and carbon tetrabromide (CBr_4, 2.17 g, 6.54 mmol) were dissolved in anhydrous dichloromethane (CH_2Cl_2, 5 mL) and then followed by stirring with ice bath for 30 min. To the mixture under stirring, triphenylphosphine (PPh_3, 1.72 g, 6.54 mmol) in CH_2Cl_2 (2 mL) was slowly added for 1 h. Then, the mixture was continuously stirred at room temperature for an additional 1 h. The reaction mixture was concentrated and then poured into cyclohexane. After filtration, the solution was concentrated and further purified by flash column chromatography with a mixture of cyclohexane and ethyl acetate (50:1 in volume). The obtained product in colorless liquid was identified in deuterated chloroform ($CDCl_3$) using Bruker nuclear magnetic resonance (NMR) spectrometers (models AV300 and AVANCE-III 600, Rheinstetten, BW, Germany) with proton (^{1}H) and carbon (^{13}C) probes. The target product, 1-bromo-10-undecyne, was obtained in 70.3% yield (0.965 g). ^{1}H NMR (300 MHz, $CDCl_3$, δ (ppm)): 3.42 (t, 2H, $-CH_2Br$), 2.20 (m, 2H, $-CH_2C{\equiv}CH$), 1.96 (t, 1H, $-CH_2C{\equiv}CH$), 1.87 (m, 2H, $-CH_2CH_2Br$), 1.60−1.25 (br, 12H, $-(CH_2)_6-$)

DOI: 10.1021/acs.macromol.7b00805
Macromolecules 2017, 50, 6489−6500

(Figure S1a in Supporting Information). ^{13}C NMR (75 MHz, $CDCl_3$, δ (ppm)): 84.8, 68.2, 34.1, 32.9, 29.4, 29.1, 28.8, 28.7, 28.6, 28.2, 18.5.

In the second step, 3β-hydroxy-Δ^5-cholenic acid (1 g, 2.67 mmol) was dissolved in anhydrous dimethylformamide (DMF, 4 mL). Cesium carbonate (Cs_2CO_3, 1.30 g, 4.00 mmol) was added to the solution, and then the mixture was stirred at room temperature for 1 h. To the mixture, 11-bromoundec-1-yne (1.40 g, 5.34 mmol) was added and followed by stirring at room temperature. After 20 h, the reaction mixture was quenched by adding $CHCl_3$ and 0.1 M HCl solution and washed with 0.1 M HCl solution and deionized, distilled water. The combined organic layers were dried over anhydrous magnesium sulfate ($MgSO_4$) and concentrated in a vacuum. The concentrated residue was purified by silica gel column chromatography with a mixture of ethyl acetate and hexane (7:3 in volume), giving the target product 1-cholenyl-10-undecyne (**R1**) in white solid. Yield: 75%. **R1** was determined to reveal two melting transitions at 13.3 and 50.7 °C in differential scanning calorimetry (DSC) analysis with 10 °C/min ramping rate. Taking into consideration the chemical structure, the first melting point at 13.3 °C could originate from the transition of crystalline state to liquid crystalline state (T_{c-lc}), where the second melting point at 50.7 °C could be assigned for the transition of liquid crystalline state to fully disordered state (T_{lc-do}). ^{1}H NMR (300 MHz, $CDCl_3$, δ (ppm)): 5.36 (m, 1H, −C═C*H*−), 4.04 (t, 2H, −COOCH_2−), 3.53 (m, 1H, −C*H*OH), 2.44−2.10 (m, 6H, −CH_2C≡CH, cholesteric acid protons), 2.05−1.91 (m, 7H, −CH$_2$C≡C*H*, cholesteric acid protons, bristle linker protons), 1.68−0.79 (m, 35H, cholesteric acid protons, bristle linker protons), 0.67 (s, 3H, −CH_3) (Figure S1b). ^{1}H NMR (300 MHz, dimethyl sulfoxide-d_6 (DMSO-d_6), δ (ppm)): 5.20 (m, 1H, −C═C*H*−), 4.55 (d, 1H, −CHO*H*), 3.92 (t, 2H, −COOCH_2−), 3.45−2.96 (m, 1H, −C*H*OH), 2.66 (t, 1H, −CH$_2$C≡C*H*), 2.34−0.77 (m, 47H, cholesteric acid protons, bristle linker protons), 0.67 (s, 3H, −CH_3) (Figure S1b). ^{13}C NMR (75 MHz, $CDCl_3$, δ (ppm)): 174.44, 140.76, 121.65, 84.74, 71.76, 68.09, 64.41, 56.72, 55.78, 50.07, 42.36, 42.28, 39.73, 37.24, 36.48, 35.34, 31.87, 31.64, 31.32, 31.04, 29.35, 29.18, 29.01, 28.71, 28.64, 28.45, 28.10, 25.92, 24.25, 21.06, 19.39, 18.39, 18.30, 11.86 (Figure S1c).

10-Undecynylphosphorylcholine (**R2**, Scheme 1) as ethyne-functionalized PC-bristle was synthesized in a two-step reaction manner according to the methods in the literature.[8−12] 10-Undecyn-1-ol (1 g, 5.94 mmol) and triethylamine (0.99 mL, 6.54 mmol) were dissolved in anhydrous tetrahydrofuran (THF, 10 mL) under a dry nitrogen atmosphere and stirred at 0 °C for 30 min. To the solution, 2-chloro-2-oxo-1,3,2-dioxaphospholane (0.60 mL, 6.54 mmol) in THF (2 mL) was added slowly for 1 h, followed by stirring at room temperature for 4 h. The reaction mixture was filtered to remove the precipitated triethylamine hydrochloride and then followed by removal of the used THF solvent at 35−40 °C using an evaporator under reduced pressure. The filtrate was put into a Smith Process vial and dissolved together with trimethylamine (1.76 g, 30.0 mmol) in anhydrous acetonitrile (20 mL). The solution was heated to 60 °C and stirred for 20 h. Then, the reaction mixture was cooled at 2 °C overnight, precipitating the target product. The precipitated product was filtered and then washed three times with acetone. The white solid product was dried and collected. Yield: 65.3% (1.293 g). **R2** was determined to exhibit a melting point at 112.0 °C (= T_m) in DSC analysis with 10 °C/min ramping rate. ^{1}H NMR (300 MHz, CD_3OD, δ (ppm)): 4.25 (br, 2H, −POCH_2CH$_2$N−), 3.88 (m, 2H, −CH_2OP−), 3.62 (m, 2H, −POCH$_2$CH_2N−), 3.21 (s, 9H, −N-(CH_3)$_3$), 2.18 (m, 3H, −CH_2C≡CH, −CH$_2$C≡C*H*), 1.72−1.58 (br, 2H, −CH_2CH$_2$OP−), 1.58−1.20 (br, 12H, −(CH_2)$_6$−) (Figure S2a). ^{13}C NMR (75 MHz, CD_3OD, δ (ppm)): 85.10, 69.54, 67.05, 66.97, 60.40, 54.67, 31.86, 30.57, 30.36, 30.12, 29.73, 29.67, 26.85, 18.99 (Figure S2b).

Poly(glycidyl azide) (PGA) was synthesized in a two-step reaction according to the method in the literature.[13−15] In the first step, poly(epichlorohydrin) (PECH) was prepared from epichlorohydrin as follows. Epichlorohydrin (40 mL, 512 mmol) was cooled to −5 °C under a nitrogen atmosphere. Triphenylcarbenium hexafluorophosphate (TCHP) (0.1 g, 0.256 mmol) was dissolved in CH_2Cl_2 and slowly added to epichlorohydrin. The mixture was stirred at room temperature for 2 days. The crude polymer in the reaction solution was purified by precipitating into MeOH several times, followed by drying in a vacuum at 40 °C for 12 h. The obtained PECH was colorless viscous liquid. Yield: 65.4% (30.921 g). ^{1}H NMR (300 MHz, $CDCl_3$, δ (ppm)): 3.89−3.49 (m, 5H, −CH_2CHO−, −CH$_2$C*H*O−, −CH_2Cl) (Figure S3a). ^{13}C NMR (75 MHz, DMSO-d_6, δ (ppm)): 78.8, 69.6, 44.1 (Figure S3b).

In the second step, PECH was converted to poly(glycidyl azide) (PGA) as follows. A mixture of PECH (1 g, 10.8 mmol) and sodium azide (2.10 g, 32.4 mmol) in DMF (40 mL) was stirred at 90 °C for 24 h. After filtration, the used DMF solvent was removed by evaporation. The residue was dissolved in $CHCl_3$ and washed three times with saturated NaCl aqueous solution. The organic layer was dried over anhydrous magnesium sulfate ($MgSO_4$) and concentrated in a vacuum, giving the product in liquid. Yield: 90.1% (0.964 g). ^{1}H NMR (300 MHz, $CDCl_3$, δ (ppm)): 3.78−3.63 (m, 3H, −CH_2CHO−, −CH$_2$C*H*O−), 3.50−3.32 (m, 2H, −CH_2N$_3$) (Figure S4a). ^{13}C NMR (75 MHz, $CDCl_3$, δ (ppm)): 78.8, 69.6, 51.8 (Figure S4b).

PGA-Chol$_m$PC$_n$ polymers were prepared from the azide−alkyne click reactions of PGA with **R1** and **R2** in various mole fractions. For typical synthetic examples, the preparations of PGA-Chol$_{50}$PC$_{50}$ polymer, PGA-Chol$_{100}$, and PGA-PC$_{100}$ were described as follows. PGA (100 mg, 1.00 mmol) and **R1** (394 mg, 0.75 mmol) in $CHCl_3$ were added to **R2** (250 mg, 0.75 mmol) in a mixture of MeOH and deionized distilled water; here the mixture of $CHCl_3$, MeOH, and water was adjusted to 4:2:1 in volume. To the solution, copper(II) sulfate pentahydrate (13 mg, 5 mol %) and sodium ascorbate (30 mg, 15 mol %) were added and then stirred at room temperature for 48 h. The resulting product was purified by dialysis in a mixture of $CHCl_3$ and MeOH for 3 day and then precipitated several times into cold diethyl ether, followed by drying in vacuum at room temperature for 1 day. The target product PGA-Chol$_{50}$PC$_{50}$ was obtained in white solid. Yield: 68.2% (361 mg). ^{1}H NMR (300 MHz, $CD_3OD/CDCl_3$, δ (ppm)): 8.00−7.40 (br, 2H, −C═C*H*− in triazole), 5.36 (m, 1H, −C═C*H*−), 4.50−3.10 (br, 10H, −CH_2CHO−, −CH$_2$C*H*O−, −CH_2−triazole in backbone), 4.26 (m, 2H, −POCH_2CH$_2$N−), 4.04 (m, 2H, −COOCH_2−), 3.85 (m, 2H, −CH_2OP−), 3.67 (m, 2H, −POCH$_2$CH_2N−), 3.46 (m, 1H, −C*H*OH), 3.25 (s, 9H, −N(CH_3)$_3$), 2.65 (m, 4H, −CH_2−triazole in bristle linker), 2.42−2.13 (m, 4H, cholesteric acid protons, bristle linker protons), 2.10−0.85 (m, 55H, cholesteric acid protons, bristle linker protons), 0.69 (s, 3H, −CH_3) (Figure S5a). ^{13}C NMR (150 MHz, $CD_3OD/CDCl_3$, δ (ppm)): 174.81, 148.31, 140.90, 122.82, 121.32, 77.95, 71.13, 68.64, 66.35, 65.79, 64.46, 63.36, 58.86, 56.69, 55.73, 54.07, 50.77, 50.08, 42.31, 41.82, 39.70, 37.23, 36.44, 35.30, 31.84, 31.80, 31.24, 31.11, 30.99, 30.77, 29.50, 29.36, 29.25, 28.58, 28.03, 25.89, 25.77, 25.56, 24.17, 20.99, 19.23, 18.18, 11.74 (Figure S5b).

PGA-Chol$_{100}$ was prepared from PGA (100 mg, 1.00 mmol) and **R1** (787 mg, 1.5 mmol) in a mixture of DMSO and $CHCl_3$ (3:1 in volume). To the PGA and **R1** mixture, copper(I) bromide (7.2 mg, 5 mol %) was added and then degassed by three freeze−pump−thaw cycles. The solution was stirred at 55 °C for 24 h, followed by distillation under vacuum. The residue was dissolved in $CHCl_3$ and then passed through aluminum oxide (activated) to remove copper catalyst. The resulting product was purified by precipitating several times into cold diethyl ether. The product was white solid. Yield: 70.5% (440 mg). ^{1}H NMR (300 MHz, $CDCl_3$, δ (ppm)): 8.00−7.40 (br, 1H, -C═C*H*- in triazole), 5.36 (m, 1H, -C═C*H*-), 4.50−3.10 (br, 5H, −CH_2CHO-, −CH$_2$C*H*O-, −CH_2-triazole in backbone), 4.04 (m, 2H, −COOCH_2-), 3.53 (m, 1H, −C*H*OH), 2.65 (m, 2H, −CH_2-triazole in bristle), 2.42−2.13 (m, 4H, cholesteric acid protons, bristle linker protons), 2.10−0.86 (m, 41H, cholesteric acid protons, bristle linker protons), 0.71 (s, 3H, −CH_3) (Figure S6a). ^{13}C NMR (150 MHz, $CDCl_3$, δ (ppm)): 173.96, 148.22, 141.01, 122.14, 121,34, 77.95, 71.61, 68.78, 64.21, 56.85, 56.02, 50.77, 50.32, 42.46, 42.43, 39.88, 37.39, 36.56, 35.28, 32.03, 31.89, 31.76, 31.37, 31.12, 29.47, 29.38, 29.31, 29.24, 27.99, 25.94, 25.71, 24.23, 21.13, 19.31, 18.35, 11.86 (Figure S6b).

DOI: 10.1021/acs.macromol.7b00805
Macromolecules 2017, 50, 6489−6500

PGA-PC_{100} was prepared from PGA (100 mg, 1.00 mmol) in $CHCl_3$ and **R2** (500 mg, 1.50 mmol) in a mixture of MeOH and deionized water; the mixture of $CHCl_3$, MeOH, and water was adjusted to 2:2:1 in volume. To the PGA and **R2** mixture, copper(II) sulfate pentahydrate (12 mg, 5 mol %) and sodium ascorbate (30 mg, 15 mol %) were added and then stirred at room temperature for 48 h. The resulting product was purified by dialysis in a mixture of $CHCl_3$ and methanol for 3 days and then concentrated under vacuum. The product was obtained in green solid. Yield: 68.4% (296 mg). ^{1}H NMR (300 MHz, $CD_3OD/CDCl_3$, δ (ppm)): 8.00−7.40 (br, 1H, −C═C*H*− in triazole), 4.50−3.10 (br, 5H, −CH_2CHO−, −CH_2C*H*O−, −CH_2−triazole in backbone), 4.26 (m, 2H, −POCH_2CH_2N−), 3.85 (m, 2H, −CH_2OP−), 3.67 (m, 2H, −POCH_2CH_2N−), 3.25 (s, 9H, −N(CH_3)$_3$), 2.65 (m, 2H, −CH_2−triazole in bristle linker), 1.90−0.85 (m, 14H, −(CH_2)$_7$−) (Figure S7a). ^{13}C NMR (150 MHz, $CD_3OD/CDCl_3$, δ (ppm)): 148.09, 123.53, 77.79, 76.64, 70.21, 68.70, 66.06, 65.49, 58.97, 53.34, 50.91, 30.62, 29.43, 29.23, 25.65, 25.29 (Figure S7b).

Thin Film Preparation. The individual polymers were dissolved in either $CHCl_3$, MeOH or $CHCl_3$/MeOH mixtures and filtered using disposable syringes equipped with polytetrafluoroethylene filter membranes of 0.22 μm pore size, producing polymer solutions with a concentration of 0.1−1.0 wt %. Each polymer solution was deposited on precleaned silicon (Si) substrates via spin-coating process and annealed with using various solvents, such as MeOH, THF, and $CHCl_3$, at room temperature for 0.5−4 h, then followed by drying in a vacuum at room temperature for 24 h. The obtained polymer films were determined to have a thickness of 60−80 nm by using a spectroscopic ellipsometer (Model M-2000, Woollam, Lincoln, NE). An average surface roughness (i.e., root-mean square roughness) was additionally measured by ellipsometry.

Measurements. Molecular weight and distribution were determined by using a gel permeation chromatography (GPC) system (model PL-GPC 210, Polymer Laboratories, Amherst, MA) equipped with two PL-Gel Mixed-C columns calibrated with polystyrene standards; in the measurements, $CHCl_3$ was used as an eluent. Thermal stability and phase transitions were measured with a rate of 10.0 °C/min under a nitrogen atmosphere by thermogravimetry (TGA; model TG/DGA-6300, Seiko Instrument, Tokyo, Japan) and differential scanning calorimetry (DSC) (model DSC-220CU, Seiko Instrument, Tokyo, Japan).

Synchrotron GIXS measurements were performed at 3C and 9A beamlines of the Pohang Accelerator Laboratory (PAL), Pohang University of Science & Technology (POSTECH)), Pohang, Korea.[16−18] Scattering data were normally collected for 10−30 s using X-ray radiation sources with a wavelength λ of 0.1117 and 0.1290 nm and a two-dimensional (2D) charge-coupled detector (CCD) (model Rayonix 2D MAR, Evanston, IL). The sample-to-detector distance (SDD) was 234.9 mm for grazing incidence wide-angle X-ray scattering (GIWAXS) measurements and 2929.6 mm for grazing incidence small-angle X-ray scattering (GISAXS) measurements. The incidence angle α_i of X-ray beam with respect to the sample specimen surface was set in the range 0.130°−0.160°, which is between the critical angle of the polymer film and the silicon substrate ($\alpha_{c,f}$ and $\alpha_{c,s}$). Scattering angles were corrected according to the positions of the X-ray beams reflected from the silicon substrate as well as by using precalibrated sucrose standard (TCI, Tokyo, Japan). Aluminum foils were used as a semitransparent beamstop because the intensity of the specular reflection from the substrate is much stronger than the intensity of GIXS near the critical angle.

X-ray photoelectron spectroscopy (XPS) measurements were carried out on an X-ray photoelectron spectrometer (model PHI 5000 Versa Probe, Ulvac-PHI, Kanagawa, Japan) with monochromatized Al Kα radiation (1486.6 eV). The pressure inside the analyzer was maintained at 2.0×10^{-7} Pa. A spot size of 100 μm × 100 μm was examined; the detection limit was 0.5 at.%. A wide scan pass energy of 117.4 eV and a narrow scan pass energy of 46.95 eV were used. The electron takeoff angle was 45° with respect to the film surface. All binding energies were referenced to the C_{1s} peak (284.6 eV) of adventitious carbon component.

Water contact angles were measured at room temperature using a contact angle meter (KSV Instruments, Tokyo, Japan). At least five sessile drops of water were measured for each polymer film to get reproducibility.

RESULTS AND DISCUSSION

In this study, we have aimed to develop a new, novel polymer system mimicking three key features (i.e., phospholipid, cholesterol, and self-assembling ability) of cell membranes. To meet this mission, we have considered poly(ethylene glycol) (PEG) as a base polymer backbone because it possesses excellent biocompatibility and thus is widely used in the biomedical fields. In general, linear PEG possesses only two hydroxyl groups at the chain ends. Because of such lack of functionality, PEG itself could not be useful for our study. Thus, we have chosen PECH, which is a functionalized PEG analogue, as a base polymer for our mission. To mimic the biofunctionality and self-assembling nature of phospholipid, we have considered the chemical combination of phosphorylcholine and functionalized alkane. And we have tried to add a self-assembling ability to the biofunctionality of cholesterol via the chemical combination of cholesterol and functionalized alkane. Finally, we have made much effort to find a best way to incorporate such phospholipid and cholesterol mimics into PECH. To achieve such chemical incorporations, there are two major possible options: (i) as a bottom-up approach, the modifications of epichlorohydrin to include phospholipid and cholesterol mimics and their copolymerization; (ii) as a top-down approach, the preparation of PECH and its post-modifications to incorporate phospholipid and cholesterol mimics. The bottom-up approach was faced to serious problems in the monomer modifications and their copolymerization due to the reactive hydroxyl group of cholesterol unit as well as the zwitterionic nature of phosphorylcholine unit. Indeed, we have decided to take the top-down approach in this study. For the top-down approach there are basically two options possible. The first option is to incorporate phospholipid and cholesterol mimics into PECH via the coupling reactions using the chloro groups of the polymer. The second option is to modify the chloro groups of PECH to other proper functional groups and use them to incorporate phospholipid and cholesterol mimics into the polymer. For the first option, we have realized some serious problems due to the presences of hydroxyl group in the cholesterol unit and relatively less stable phosphate linkage in the phosphorylcholine unit as well as the quite different solubility nature between cholesterol and phosphorylcholine units. In comparison, the second option has more flexibility in finding proper chemical reactions and their conditions. As a result of these efforts, we have developed an ethyne-functionalized alkane containing cholesterol, an ethylene-functionalized alkane bearing phosphorylcholine, and a fully azide-functionalized PECH, namely PGA. From these materials, we have finally succeeded to synthesize a well-defined brush random copolymer mimicking the three key features of cell membranes.

1-Cholenylundec-10-yne (**R1**, ethyne-functionalized Chol-bristle) as a cholesterol mimic was synthesized from 10-undecyn-1-ol in a two-step reaction manner, as shown in Scheme 1. 10-Undecyn-1-ol was converted to 11-bromoundec-1-yne in a reasonably high yield via the reaction with CBr_4 with the aid of PPh_3 catalyst. 11-Bromoundec-1-yne was further reacted with 3β-hydroxy-Δ^5-cholenic acid in the aid of Cs_2CO_3, producing **R1** in a good yield (Figure S1).

DOI: 10.1021/acs.macromol.7b00805
Macromolecules 2017, 50, 6489−6500

Table 1. Characteristics of the Synthesized Brush Polymers

			composition[c]		thermal properties			nanoscale thin film			
									composition at film surface[h]		
polymer	M_w[a]	PDI[b]	chol-bristle (mol %)	PC-bristle (mol %)	T_d[d] (°C)	T_g[e] (°C)	T_m[f] (°C)	surface roughness[g] (nm)	Chol-bristle (mol %)	PC-bristle (mol %)	water contact angle[i] (deg)
PECH	38500	1.68			300	−33					
PGA					195	−38					
PGA-$Chol_{100}$			≥99	0	280	82	121	0.43	100.0	0.0	96.8 (0.5)[k]
PGA-$Chol_{75}PC_{25}$			76	24	270	95	171	0.25	78.8	21.2	77.8 (0.7)
PGA-$Chol_{50}PC_{50}$			48	52	240	85	165	1.01	59.0	41.0	61.2 (0.8)
PGA-$Chol_{25}PC_{75}$			24	76	230	−16 to 92[j]		0.97	31.2	68.8	59.7 (0.7)
PGA-PC_{100}			0	≥99	230	−7 to 125[j]		0.41	0.0	100.0	soluble

[a]Weight-average molecular weight determined by GPC analysis. [b]Polydispersity index determined by GPC analysis. [c]Determined by ^{1}H NMR spectroscopy analysis. [d]Onset degradation temperature measured by TGA analysis. [e]Glass transition temperature (middle point) measured by DSC analysis. [f]Melting transition temperature (at the maximum of endothermic peak) measured by DSC analysis. [g]Root-mean-square roughness determined by spectroscopic ellipsometry. [h]Calculated from the atomic concentration ratio of P and C based on the P_{2p} and C_{1s} peaks measured for the film surface by XPS. [i]Measured at room temperature. [j]Transition range. [k]Standard deviation.

10-Undecynylphosphorylcholine (**R2**, ethyne-functionalized PC-bristle) as a phospholipid mimic was synthesized, as shown in Scheme 1. 10-Undecyn-1-ol was reacted with 2-chloro-2-oxo-1,3,2-dioxaphospholane in the first step and then treated with trimethylamine in the second step, producing **R2** in a reasonably good yield. After the reaction was completed, the unreacted 10-undecyn-1-ol could not be removed easily from the target product **R2** through conventional distillation under reduced pressure because of its high boiling point. Acetonitrile was found to be a good solvent to dissolve either both the unreacted 10-undecyn-1-ol and the target product or only one of them depending on the temperature. In this solvent, **R2** was soluble at 60 °C but insoluble at 2 °C, whereas 10-undecyn-1-ol was completely soluble over the temperature range 0−60 °C. Using the temperature-dependent solubility differences, **R2** was successfully purified (Figure S2).

With **R1** and **R2** a series of the PGA-$Chol_mPC_n$ polymers in various compositions were synthesized in a three-step manner, as shown in Scheme 1, as a novel brush random copolymer system mimicking three key features (phospholipid, cholesterol, and self-assembling ability) of cell membranes. In the first step, epichlorohydrin was undergone cationic ring-opening polymerization with the aid of TCHP initiator, producing PECH, a base polymer. PECH was identified by ^{1}H and ^{13}C NMR spectroscopy analysis (Figure S3). This base polymer was characterized to have a weight-average molecular weight ($\overline{M}_w$) of 38 500 and a polydispersity index (PDI) of 1.68 by GPC analysis (Figure S8).

In the second step, PECH was converted to PGA via the reaction of the chloro side groups with sodium azide. The ^{1}H and ^{13}C NMR and FTIR spectroscopy analyses confirmed that all chloro groups of PECH were completely replaced by azido groups (Figures S3, S4, and S9). In particular, the IR spectroscopy analysis confirmed that the vibrational characteristic band at 750 cm^{-1} of the $-CH_2-Cl$ groups of PECH completely disappeared while the incorporated azido groups newly appeared at 2100 cm^{-1} as a very strong vibrational band (Figure S9a,b).

In the last step, PGA was undergone azide−alkyne click reaction with **R1** and **R2** in various compositions, producing the target PGA-$Chol_mPC_n$ polymers. For conducting this reaction we have been faced to a serious problem. The problem was caused from the significantly different chemical natures in solvent of **R1** having an amphiphilicity, **R2** possessing both an amphiphilicity and a zwitterionic characteristic, and PGA with a weak amphiphilicity. As a result of testing a number of solvent systems, a mixture of $CHCl_3$, MeOH, and deionized distilled water (4:2:1 in volume) was found as a best solvent system for all components in the click reaction. But there were required special cares for making such cosolvent system as follows. At the first, **R1** and PGA were dissolved in $CHCl_3$ while **R2** was dissolved in a small amount of MeOH. Then the **R2** solution was added into the solution of **R1** and PGA under stirring. When the addition was completed, the mixture appeared turbid. Thus, more MeOH was added to the mixture until the turbidity disappeared, followed by adding a proper amount of water. Because of the cosolvent containing water, we additionally chose copper(II) sulfate pentahydrate combined with sodium ascorbate as a catalyst system, rather than copper(I) bromide being widely used in organic solvents. After the click reaction was completed, the target brush polymer products were purified through the two steps as follows. **R2** in excess and the used catalyst components were removed out from the reaction mixture by dialysis in water for 3 days. The residues were again dissolved in a mixture of chloroform and methanol and poured into diethyl ether in an ice water bath, precipitating the brush polymer product. The precipitate was filtered and again dissolved in a mixture of chloroform and methanol. The solution was poured into cold diethyl ether, precipitating the polymer product. The precipitate was filtered and dried, giving the target brush polymer. In similar manner, PGA-PC_{100} was synthesized from PGA and **R2**. In comparison, PGA-$Chol_{100}$ was prepared in a mixture of DMSO and $CHCl_3$ (3:1 in volume) from PGA and **R1** with the aid of copper(I) bromide rather than copper(II) sulfate pentahydrate/sodium ascorbate.

All brush polymer products were identified by NMR and IR spectroscopy analyses (Figures S5, S6, S7, and S9). In particular, the vibrational peak of the azido groups at 2100 cm^{-1} disappeared completely, but the chemical shift of the azide−alkyne click reaction product triazolyl linkages (−C=C*H*−) newly appeared at 8.00−7.40 ppm. These results

DOI: 10.1021/acs.macromol.7b00805
Macromolecules 2017, 50, 6489−6500

confirmed that all azido groups of PGA were completely undergone click reactions with **R1** and/or **R2**. For each brush polymer product, the chemical composition, namely the molar fraction of Chol- and PC-bristles, was determined by analyzing the integrals of the chemical shifts at 8.00−7.40 ppm (−C═C*H*− in triazole), 5.36 ppm (−C═C*H*− in Chol-bristle), 3.25 ppm (−POCH$_2$C*H*$_2$N− in PC-bristle), and 2.65 ppm (−C*H*$_2$− triazole in bristle) in the ^{1}H NMR spectrum. The obtained chemical compositions are summarized in Table 1.

PGA-Chol$_{100}$ was thermally stable up to 280 °C (= T_d, onset degradation temperature). PGA-PC$_{100}$ revealed T_d = 230 °C. The relatively lower thermal stability of PGA-PC$_{100}$ may be attributed to the presence of phosphate linkage in the bristle. The PGA-Chol$_m$PC$_n$ polymers exhibited T_d over the range 230−270 °C; the copolymer bearing higher Chol-bristle content showed higher T_d (Figure 1a and Table 1). All brush

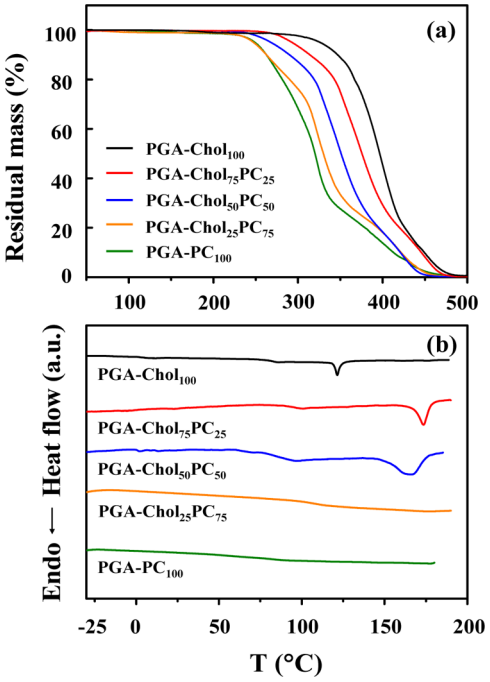

Figure 1. (a) TGA and (b) DSC thermograms of PGA-Chol$_m$PC$_n$ polymers, which were measured at a rate of 10.0 °C/min under a nitrogen atmosphere.

random copolymers revealed excellent solubility in common organic solvents ($CHCl_3$, MeOH, DMF, DMSO, etc.), giving good quality films (0.25−1.01 nm surface roughness) in conventional solution casting processes (Table 1). In particular, PGA-PC$_{100}$ was soluble in water.

Nanoscale thin films (60−80 nm thick) of the PGA-Chol$_m$PC$_n$ polymers were investigated by synchrotron GIXS analysis. The as-cast films were confirmed to reveal poorly developed structures. Thus, the as-cast films were undergone to anneal with the aids of various solvents (MeOH, THF, and $CHCl_3$) to achieve more ordered morphological structures. As shown in Figure S10, the brush polymers revealed more featured GIXS images in the films annealed with MeOH rather than the other solvents. These results inform that the brush polymers tend to form higher ordered and oriented morphology structures in the MeOH-annealed films rather than in the other solvent-annealed films. With these results, the MeOH-annealing process was further optimized. Figure 2

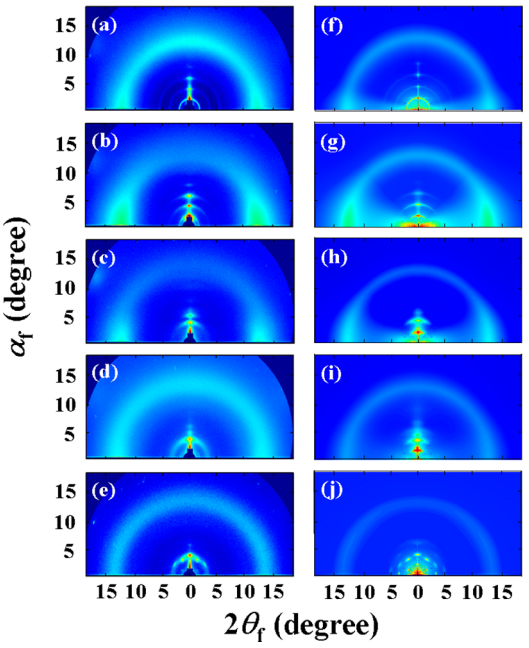

Figure 2. 2D GIWAXS patterns of PGA-Chol$_m$PC$_n$ polymers in thin films which were measured with SDD = 234.9 mm using an X-ray beam with λ = 0.1117 nm: (a) PGA-Chol$_{100}$ (α_i = 0.141°); (b) PGA-Chol$_{75}$PC$_{25}$ (α_i = 0.150°); (c) PGA-Chol$_{50}$PC$_{50}$ (α_i = 0.150°); (d) PGA-Chol$_{25}$PC$_{75}$ (α_i = 0.150°); (e) PGA-PC$_{100}$ (α_i = 0.156°). 2D scattering patterns reconstructed with the determined structural parameters (Table 2) using the GIXS formulas derived for lamellar and orthorhombic cylinder structure models (Supporting Information): (f) PGA-Chol$_{100}$; (g) PGA-Chol$_{75}$PC$_{25}$; (h) PGA-Chol$_{50}$PC$_{50}$; (i) PGA-Chol$_{25}$PC$_{75}$; (j) PGA-PC$_{100}$.

shows representatives of the measured 2D GIWAXS patterns of the polymer films, which were annealed with MeOH at room temperature for 4 h, then followed by drying in a vacuum at room temperature for 24 h. Their one-dimensional (1D) profiles are shown in Figure 3, which were extracted along the α_f direction at $2\theta_f$ = 0° and along the $2\theta_f$ direction at α_f = 0.160°; here α_f and $2\theta_f$ are the out-of-plane and in-plane exit angle of the X-ray scattering beam, respectively.

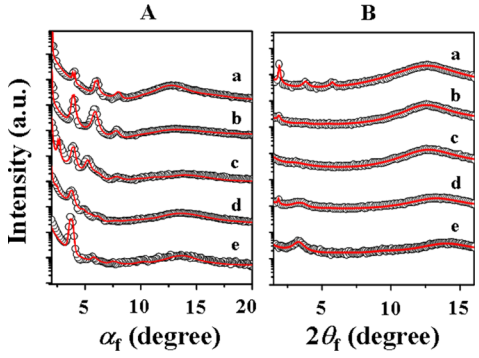

Figure 3. (a) Out-of-plane and (b) in-plane scattering profiles extracted along the α_f direction at $2\theta_f$ = 0° and $2\theta_f$ direction at α_f = 0.160°, respectively, from the 2D scattering patterns in Figure 2a−e. The open circles are the measured data points, and the red solid lines were obtained by fitting the data with the GIXS formulas derived for lamellar and orthorhombic cylinder structure models (Supporting Information).

DOI: 10.1021/acs.macromol.7b00805
Macromolecules 2017, 50, 6489−6500

Table 2. Structural Parameters of PGA-Chol$_m$PC$_n$ Polymers in Thin Films Determined by Quantitative GIXS Analysis

	PGA-Chol$_{100}$	PGA-Chol$_{75}$PC$_{25}$	PGA-Chol$_{50}$PC$_{50}$	PGA-Chol$_{25}$PC$_{75}$		PGA−PC$_{100}$	
structural parameter	lamellar structure	lamellar structure	lamellar structure	pseudo-lamellar structure	lamellar structure	pseudo- lamellar structure	orthorhombic cylindrical structure
d_L (nm)[a]	3.18	3.25	3.25	2.44	3.37	2.62	
d_1 (nm)[b]	1.82 (0.08)[z]	1.83 (0.21)	0.98 (0.10)	0.64 (0.05)	1.00 (0.13)	0.80 (0.10)	
d_2 (nm)[c]	1.36	1.42	2.27	1.80	2.37	1.82	
d_{r1} (nm)[d]	0.51	0.50	0.50	0.50	0.49	0.49	
d_{r2} (nm)[e]	0.62	0.58	0.58	0.58	0.56	0.56	
d_{r3} (nm)[f]	0.81	0.81	0.81	0.81	0.81	0.81	
g_{33}[g]	0.06	0.06	0.08	0.08	0.08	0.08	
g_{rr}[h]	0.01	0.01	0.01	0.01	0.01	0.01	
$\bar{\varphi}$ (deg)[i]	0 (4.20)	0 (5.99)	0 (9.17)		0 (10.94)		
O_S[j]	0.992	0.984	0.963		0.947		
$\phi_{L,h}$ (%)[k]	62	100	51	49	53	47	
$\phi_{L,v}$ (%)[l]	19						
$\phi_{L,r}$ (%)[m]	19						
d_v (nm)[n]							3.43
d_h (nm)[o]							5.16
R_v (nm)[p]							2.15
$R_{c,v}$ (nm)[q]							0.48 (0.05)
$R_{s,v}$ (nm)[r]							1.67 (0.30)
R_h (nm)[s]							2.58
$R_{c,h}$ (nm)[t]							1.00 (0.03)
$R_{s,h}$ (nm)[u]							1.58 (0.21)
g[x]							0.07
d_{r1} (nm)[y]							0.48
$\bar{\varphi}$ (deg)[i]							0 (3.31)
O_S[j]							0.995

[a]Long period. [b]Thickness of denser sublayer. [c]Thickness of less dense sublayer. [d]Mean interdistance between the nearest bristles. [e]Mean interdistance between the nearest backbones. [f]Mean interdistance between the nearest bristles along the polymer backbone. [g]Paracrystal distortion factor along a direction normal to the in-plane of multibilayer structure. [h]Paracrystal distortion factor of the bristles along the lateral packing direction. [i]Mean polar angle (that is orientation angle) between the orientation n vector of nanostructure (horizontal multibilayer structure or horizontal OPC structure) and the out-of-plane direction of the film. [j]Second-order orientation factor. [k]Relative volume fraction of horizontal multibilayer structure. [l]Relative volume fraction of vertical multibilayer structure. [m]Relative volume fraction of randomly oriented multibilayer structure. [n]Mean interdistance between the stacks of the horizontal cylinder arrays. [o]Mean center-to-center distance in the horizontal cylinder array. [p]Mean height of core−shell ellipsoidal cylinder. [q]Mean height of the core part of core−shell ellipsoidal cylinder. [r]Mean height of the shell part of core−shell ellipsoidal cylinder. [s]Mean width of core−shell ellipsoidal cylinder. [t]Mean width of the core part of core−shell ellipsoidal cylinder. [u]Mean width of the shell part of core−shell ellipsoidal cylinder. [x]Positional distortion factor of core−shell ellipsoidal cylinders. [y]Mean interdistance between the nearest bristles along the polymer backbone. [z]Standard deviation.

The PGA-Chol$_{100}$ film revealed four weak scattering rings (i.e., semicircular rings) with a regular angle interval: 2.01°, 4.03°, 6.03°, and 8.05° (Figure 2a). In addition, a set of scattering spots appeared with a regular angle interval along the α_f direction at $2\theta_f = 0°$; the positions in scattering angle of the individual spots were well matched with those of the four weak scattering rings (Figures 2a and 3A-a). The first three of such four scattering spots were also discernible weakly along the $2\theta_f$ direction at $\alpha_f = 0°$ or 0.160° (Figures 2a and 3B-a). The scattering peaks were found to have relative scattering vector lengths from the specular reflection position of 1, 2, 3, and 4, indicating that they are in a relationship of the first-, second-, third-, and fourth-order scattering peaks originating from a same reflection plane. These results collectively inform that lamellar structures in three different orientations are present in the film; namely, horizontally oriented lamellae were formed as a major structural component while vertically and randomly oriented lamellae were formed as minor structural components. The relative fractions of the lamellae in such orientations were estimated by the quantitative analysis of the azimuthal scattering profile extracted at 6.03° (Figure S11): 62% horizontally oriented lamellar structure (= $\phi_{L,h}$), 19% vertically oriented lamellar structure (= $\phi_{L,v}$), and 19% randomly oriented lamellar structure (= $\phi_{L,r}$). The polymer film showed an additional scattering around 12.58°, which was broad and weak. In fact, this scattering ring is anisotropic rather than isotropic. Its intensity is relatively stronger along the meridian direction and much stronger along the equatorial direction. Its d-spacing was estimated to be 0.51 nm (= d_{r1}). Taking into consideration the chemical structure and lamellar structure formation characteristics of the brush polymer, the d_{r1} value can be assigned to the mean interdistance between the nearest bristles in extended conformation. With these results, the GIXS pattern was further analyzed in a quantitative manner by using the GIXS formula derived for a lamellar structure model composed of two sublayers; details of the GIXS formula are given in the Supporting Information. The out-of-plane and in-plane scattering profiles were successfully well fitted with the GIXS formula, as shown in Figures 3A-a and 3B-a. In particular, the azimuthal scattering profile extracted at 4.03° was analyzed in order to get orientation details of the horizontal lamellar

DOI: 10.1021/acs.macromol.7b00805
Macromolecules 2017, 50, 6489−6500

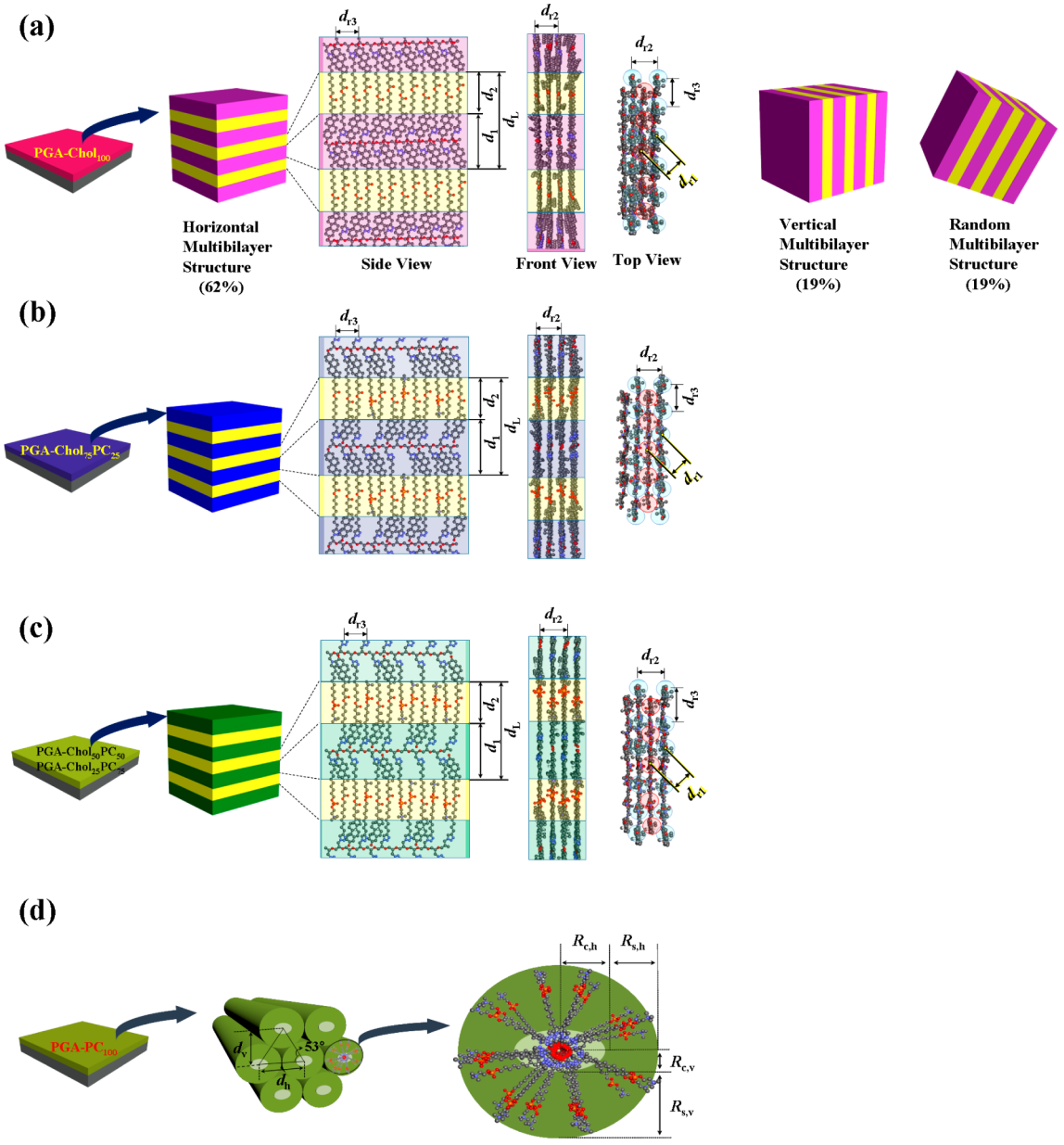

Figure 4. Schematic representations of molecular chain conformations and packing orders in films of PGA-Chol$_m$PC$_n$ polymers: (a) PGA-Chol$_{100}$; (b) PGA-Chol$_{75}$PC$_{25}$; (c) PGA-Chol$_{50}$PC$_{50}$ and PGA-Chol$_{25}$PC$_{75}$; (d) PGA-PC$_{100}$.

structure (Figure S12a). The GIXS analysis results are summarized in Table 2.

The GIWAXS analysis results collectively inform that the PGA-Chol$_{100}$ molecules favorably self-assemble, forming lamellar structure with characteristic features in the following. The long period d_L is 3.18 nm, which consists of a denser sublayer of 1.82 nm thick (= d_1) and a less dense sublayer of 1.36 nm thick (= d_2). The base polymer PECH of PGA-Chol$_{100}$ is known fully amorphous. The d_L value is close to the length of the bristles in fully extended conformation. The d_1 value is close to twice the length of the cyclic parts in the cholesterol unit of the Chol-bristle. Taking these facts into account, the lamellar structure in the film might result from the favorable self-assembling, namely lateral packing of the Chol-bristles in extended conformation. In the lamellar structure, the bristles might be completely interdigitated between the lamellae in contact along the stacking direction. Such complete interdigitation and lateral packing of the Chol-bristles could be feasible when the polymer backbone chains behave extended conformation, namely 2_1 conformation. Because of the complete interdigitated bristles, the lamellar structure can be classified as a multibilayer structure. Considering this interdigitation characteristic and the chemical structure, the denser sublayer is made of the interdigitated cyclic parts, the triazolyl units with inner parts of the alkylenyl linkers, and the polymer backbones; the less dense sublayer is made of the rest parts of the alkylenyl linkers. In fact, the formation of this multibilayer structure is remarkable in regard to some obstacles such as the triazolyl unit causing a kink and the bulky cyclic cholesterol part in the Chol-bristle. It turns out that the self-assembling ability of the Chol-bristle overrides possible negative contributions of the triazolyl kink and bulky cyclic cholesterol part, leading to the formation of multibilayer structure. The multibilayer structure is formed in a mixture of

DOI: 10.1021/acs.macromol.7b00805
Macromolecules 2017, 50, 6489−6500

horizontal, vertical, and random orientations. In particular, the horizontal multibilayer structure is formed as the major structural component. Its positional distortion factors (g_{33} and g_{rr}) are very small, 0.01−0.06, indicative of high dimensional stability of the horizontal multibilayer structure. Furthermore, the structure reveals high second order orientation factor O_s (0.992) where the mean polar angle $\bar{\varphi}$ is 0° and the deviation of polar angle $\sigma_\varphi$is 4.20°. Taking into account the multibilayer structure with the complete interdigitation of extended bristles, we could further estimated the mean interdistance between the nearest backbones (= d_{r2}) and the mean interdistance between the nearest bristles along the polymer backbone (= d_{r3}) from the mean interdistance of the nearest bristles (d_{r1} = 0.51 nm) determined from the scattering ring at 12.58°. From the structural details determined above, the molecular chain conformation and self-assemblies of PGA-Chol$_{100}$ in the film could be drawn in a schematic manner, as shown in Figure 4a.

Surprisingly, a quite different scattering pattern was observed for PGA-PC$_{100}$ in films. As shown in Figure 2e, the PGA-PC$_{100}$ film reveals several scattering spots in the angle region of <6° and a relatively broad, isotropic scattering ring at 13.35°. Two spots appear at 3.75° (1.71 nm *d*-spacing) and 5.64° (*d* = 1.14 nm) along the meridian line. These spots were estimated to have relative scattering vector lengths from the specular reflection position of 2 and 3, indicating that they are the second- and third-order scattering peaks originating from a same reflection plane. The first-order peak of these spots is expected to appear at 1.88° (*d* = 3.43 nm), which is heavily overlapped with the parasitic scattering from the reflected main X-ray beam. The observation of these spots suggests that in the film arrays with a mean interdistance of 3.43 nm are present along a direction normal to the film plane. Three scattering spots additionally appear in the out of meridian line. One weak scattering spot is discernible at α_f = 1.42° and $2\theta_f$ = 1.05° (*d* = 3.61 nm) while another scattering spot is shown at α_f = 2.88° and $2\theta_f$ = 2.19° (*d* = 1.79 nm). Their relative scattering vector lengths from the specular reflection position are 1 and 2, indicating that they are the first- and second-order scattering peaks originating from a same reflection plane. A relatively strong spot appears at α_f = 3.06° and $2\theta_f$ = 1.42° (*d* = 1.90 nm). All scattering spots could be assigned with taking into consideration horizontally oriented cylinders and their closed packing lattice (i.e., hexagonal lattice), as shown in Figure S13; the (01), (02), (03), (10), (20), and (11) reflections appear. However, both the (10) and (20) reflections (α_f = 1.42° and $2\theta_f$ = 1.05° and at α_f = 2.88° and $2\theta_f$ = 2.19°) are found to position at an azimuthal angle μ of 37° rather than 30°, suggesting that in the film the horizontal cylinders formed a hexagonally packed cylinder (HPC) structure with a certain degree of distortion, rather than a regular HPC structure. The out-of-plane and in-plane scattering profiles could be successfully fitted by using the GIXS formula derived with an orthorhombic lattice model (which is a distorted HPC lattice) consisting of elliptical cylinders with two phases (Figures 3A−e and 3B−e); the details of GIXS analysis are given in the Supporting Information. In addition, the azimuthal scattering profile extracted at 3.95° was analyzed in detail (Figure S12e). The broad, isotropic scattering ring at 13.35° is estimated to have a small *d*-spacing value, 0.48 nm. Considering such small *d*-spacing value, the scattering ring might originate from the mean interdistance of the nearest-neighbored bristles (= d_{r1}). The analysis results are listed in Table 2.

The orthorhombically packed cylinder (OPC) structure formed in the PGA-PC$_{100}$ film is characterized with key features as follows. The individual cylinders are preferentially oriented in the film plane, elliptic, and consist of two phases, namely a core part and a shell part; R_v = 2.15 nm (radius in the out-of-plane direction, namely short radius): $R_{c,v}$ = 0.48 nm (core radius) and $R_{s,v}$ = 1.67 nm (shell thickness); R_h = 2.58 nm (radius in the in-plane direction, namely long radius): $R_{c,h}$ = 1.00 nm (core radius) and $R_{s,h}$ = 1.58 nm (shell thickness). The cross section of the cylinders is comparable to that of a single PGA-PC$_{100}$ chain in helical conformation, suggesting that each cylinder is made of a single helical PGA-PC$_{100}$ chain. Taking into consideration the helical conformation and chemical structure of PGA-PC$_{100}$, the core part with a relatively higher electron density of the elliptic cylinder could be composed of the triazolyl units, polymer backbone, and inner parts of the alkylenyl linkers in the bristles, whereas the shell part could consist of the PC end groups and outer parts of the alkylenyl linkers in the bristles. The mean center-to-center distance of the cylinders lain in a direction parallel to the film plane is 5.16 nm (= d_h). The mean interdistance between the stacks of the horizontal cylinder arrays is 3.43 nm (= d_v). The d_v/d_h ratio is calculated to be 0.665, which is somewhat far from that (= $\sqrt{3}/2$) for a regular HPC structure. This d_v/d_h ratio value again confirms that the horizontal helical PGA-PC$_{100}$ cylinders were closely packed together, forming a highly distorted HCP structure, namely OPC structure. The positional distortion factor *g* is very small, 0.07, whereas the orientation factor O_s is 0.995 with $\bar{\varphi}$ = 0° and its standard deviation $\sigma_\varphi$is 3.31°. These factors are the evidence that the OPC structure formed in the film is well oriented in the film plane and very stable dimensionally. Taking into account the dimensional parameters of the molecular cylinder in the OPC structure and the d_{r1} value, the molecular PGA-PC$_{100}$ cylinder has been confirmed to behave 12_5 helical conformation by molecular simulations using the Cerius^2 software package (Accelrys, San Diego, CA). From the structural analysis details above, schematic representations of the molecular chain conformation and self-assemblies of PGA-PC$_{100}$ in the film could be depicted, as shown in Figure 4d.

Quantitative GIWAXS analysis was extended for the scattering patterns of PGA-Chol$_{75}$PC$_{25}$, PGA-Chol$_{50}$PC$_{50}$, and PGA-Chol$_{25}$PC$_{75}$ films. The analysis results are presented in Table 2, Figure 3, and Figure S12. These brush random copolymers in films were confirmed to form only horizontal multibilayer structures rather than orientationally mixed multibilayer structures. However, their structural dimension parameters were found to vary somewhat with the chemical compositions. As the content of Chol-bristle is decreased, d_L as well as d_2 is discernibly increased, whereas d_1 is decreased. In cases of PGA-Chol$_{50}$PC$_{50}$ and PGA-Chol$_{25}$PC$_{75}$ films, horizontally oriented pseudo-lamellar structure (namely, slightly less ordered multibilayer structure) was found to form in addition to the more ordered multibilayer structure (Figure S14). The pseudo-multibilayer structures reveal relatively smaller dimensional parameters than those of the more ordered multibilayer structures. These dimensional changes as well as the additional pseudo-multibilayer structure formations might be attributed to compositional inhomogeneities of the bristles that make critical roles in the self-assembly structure formation. In fact, the length of the PC-bristle is relatively shorter than that of the Chol-bristle. Taking this fact into account, the more ordered multibilayer structures behaving a relatively larger d_L value

DOI: 10.1021/acs.macromol.7b00805
Macromolecules 2017, 50, 6489−6500

might be made of the polymer chain parts enriched with Chol-bristles, whereas the pseudo-multibilayer structures revealing a relatively smaller d_L value might be formed with the polymer chain parts enriched by PC-bristles and/or their mixture with Chol-bristles. Taking into account the structural details in Table 2, schematic representations of the molecular chain conformation and self-assemblies of PGA-Chol$_m$PC$_n$ copolymers in the film could be given, as presented in Figures 4b,c.

The brush polymer films were additionally examined by GISAXS analysis. However, they showed featureless GISAXS patterns (see some representative images in Figure S15), suggesting that no discernible microstructures were formed in the films.

For the brush polymer films, XPS analysis was conducted in order to get information on the chemical composition at the film surface. Considering atomic components of the polymers, P and C elements were measured; P_{2p} and C_{1s} spectra were obtained, as shown in Figure S16. For each film data, quantitative XPS analysis was performed by the determination of P_{2p} and C_{1s} peak areas corrected with the relative sensitivity factors (0.525 for P_{2p} and 0.314 for C_{1s}). As a result, the concentration ratio of P and C atomic components at each film surface was obtained from the P_{2p} and C_{1s} peak areas. From the P and C atomic concentration ratios, the composition ratios of Chol- and PC-bristles were calculated. The content of PC-bristle at the film surface was obtained to be 0 mol % for the PGA-Chol$_{100}$ film, 21.2 mol % for the PGA-Chol$_{75}$PC$_{25}$ film, 41.0 mol % for the PGA-Chol$_{50}$PC$_{50}$ film, 68.8 mol % for the PGA-Chol$_{25}$PC$_{75}$ film, and 100 mol % for the PGA-PC$_{100}$ film; from the results, the Chol-bristle contents at the film surfaces were further estimated (Table 1). Overall, the XPS analysis confirmed the presence of PC bristles at the copolymer film surfaces. The PC-bristle content at the film surface was increased with its chemical loading into the copolymer. However, the PC-bristle content of each copolymer at the film surface is slightly lower than that determined by NMR spectroscopy analysis (Table 1). Such lower contents of PC-bristle at the film surfaces might be mainly attributed to the multibilayer structures consisted of vertically oriented bristles in which the PC-bristle is ca. 0.74 nm shorter in length than the Chol-bristle. Also, such discrepancies might be caused in part from the differences in the sensitivities and resolutions of XPS and NMR spectroscopy analyses.

The brush polymer films were further subjected to water contact angle measurements. The results are listed in Table 1. The PGA-Chol film exhibits a high contact angle, 96.8°. For the PGA-Chol$_m$PC$_n$ films, the water contact angle is decreased to 59.7° from 96.8° as the PC-bristle content is increased. The PGA-PC film is expected to reveal a water contact angle lower than that (59.7°) of the PGA-Chol$_{25}$PC$_{75}$ film. However, its water contact angle could not be measured because it was soluble in water.

These water contact angle results can be understood with considering the thin film morphologies discussed above. The water contact angle of PGA-Chol films is about 14° lower than that (110.7°) of poly(oxy(decyltriazolylmethyl)ethylene) (PGA-C$_{10}$) films which also reveal horizontal multibilayer structure (Figure S17) in which the surface is enriched with nonpolar methyl end groups. In general, the methyl group is more nonpolar than that of hydroxyl group. Taking this fact into account, the relatively lower water contact angle of the PGA-Chol film could be attributed to the film surface enriched with the hydroxyl end groups in the Chol-bristles in support with the multibilayer structures formed in the film. Higher PC-bristle content in PGA-Chol$_m$PC$_n$ films exhibited lower water contact angle, which could result from higher water affinity of the zwitterionic PC-bristles in structural support with the multibilayer structures formed in the films.

Self-assembling PGA-Chol$_m$PC$_n$ polymers and their homopolymers were further investigated in bulk state by DSC analysis. The measured DSC thermograms are shown in Figure 1b and Table 1. PGA-Chol$_{100}$ reveals two phase transitions: A glass transition weakly appears at 82 °C (= T_g, glass transition temperature at the middle point of the transition), and a melting transition is observed at 121 °C (= T_m, melting temperature at the transition peak maximum). PECH and PGA (which are the base polymers for PGA-Chol$_{100}$) were found to be completely amorphous, revealing T_g = −33 and −38 °C (Table 1 and Figure S18). Taking these facts into account, the relatively high glass transition is originated from the Chol-bristles bearing rigid triazolyl linker and rigid, bulky cholesterolyl moiety. Regarding the chemical structure and components, the observed T_m value seems too high. This high T_m value might be attributed to the multibilayer structure with partially interdigitated Chol-bristles discussed above.

Glass and melting transitions are also observed for PGA-Chol$_{75}$PC$_{25}$ and PGA-Chol$_{50}$PC$_{50}$. Surprisingly, both of the copolymers, however, exhibit higher T_g as well as much higher T_m, respectively, compared to those of PGA-Chol$_{100}$; in particular, PGA-Chol$_{75}$PC$_{25}$ shows the highest T_g as well as the highest T_m. In contrast, PGA-Chol$_{25}$PC$_{75}$ shows only a broad, weak transition over 55−95 °C. These results collectively inform that the PC-bristles make critical roles for multibilayer structure formation in the PGA-Chol$_m$PC$_n$ copolymer. In fact, the cholesterolyl moiety is bulky, and thus the lateral packing efficiency of the Chol-bristles may not be high in the multibilayer structure formation. Such limited lateral packing could be solved in a constructive way by aids of the less bulky, zwitterionic PC-bristles in the copolymer that are able to relieve steric hindrances present between the Chol-bristles. The results suggest that such positive, constructive contribution to the Chol-bristles' packing and resulting multibilayer structure formation could be achievable over the PC-bristle content of ≤50 mol %. However, the PC-bristle content of >50 mol % causes negative contributions on the Chol-bristles' packing and resulting multibilayer structure formation. These contributions of the PC-bristle are discernible in the GIWAXS patterns, as shown in Figure 2; PGA-Chol$_{75}$PC$_{25}$ and PGA-Chol$_{50}$PC$_{50}$ in thin films revealed a more distinguishable and intense X-ray scattering pattern, respectively, and however, PGA-Chol$_{25}$PC$_{75}$ showed a less distinguishable and weak scattering pattern compared to that of PGA-Chol$_{100}$.

Interestingly, PGA-PC$_{100}$ exhibits only a broad, weak transition. A broad, weak transition is also observed for PGA-Chol$_{25}$PC$_{75}$, as mentioned above. These phase transitions are exceptionally too broad. PGA-PC$_{100}$ was confirmed to have a helical conformation and self-assemble, forming OPC structure in films, as discussed above. On the other hand, PGA-Chol$_{25}$PC$_{75}$ was found to have an extended conformation and self-assemble, forming multibilayer structure in films; but the perfectness and overall crystallinity of the structure are relatively low. These structural features may have resulted from the zwitterionic nature of the PC-bristles that causes repulsive interactions rather than attractive interactions when they are in close contact. Such repulsive interaction characteristics of the PC-bristles could cause a significant reduction of

DOI: 10.1021/acs.macromol.7b00805
Macromolecules 2017, 50, 6489−6500

cohesive energy gain in the OPC structure formation with helical PGA-PC_{100} chains as well as in the multibilayer structure formation with PGA-$Chol_{25}PC_{75}$ chains in extended conformation. Therefore, the single broad, weak transitions observed in PGA-PC_{100} and PGA-$Chol_{25}PC_{75}$ might originate from the order−disorder transitions of such self-assembled structures with low cohesive energies in addition to the glass transitions.

CONCLUSIONS

In this study a series of well-defined PGA-$Chol_mPC_n$ polymers was successfully synthesized as a novel cell membrane mimicking system. This study demonstrated that the azide−alkyne click chemistry is a very powerful tool to effectively incorporate even bulky, heavy biomolecules as well as zwitterionic biomolecules into a polymer as side groups or bristles in a controlled, well-defined manner. The cell membrane mimicking polymers were found to be soluble in common solvents, showing good solution processability. They were thermally stable up to 230 °C or higher temperatures, depending on the bristle compositions.

Morphology details of the cell membrane mimicking polymers in nanoscale thin films were investigated by synchrotron GIXS analysis. Very interestingly, all PGA-$Chol_mPC_n$ polymers as well as PGA-$Chol_{100}$ favorably formed multibilayer structures with 2_1 chain conformation, whereas PGA-PC_{100} formed OPC structure with 12_5 helical chain conformation. Such multibilayer structure formations could be driven by a strong self-assembling ability of the Chol-bristle in extended conformation which overrides possible obstacles such as the kink unit caused by trizolyl unit and the bulky cholesterol unit in the bristle. In comparison, the OPC structure formation could be driven by a lateral packing ability of the brush polymer chain in the helical confirmation resulted from the minimization of repulsive interactions in the neighbored zwitterionic PC-bristles. The GIXS and DSC analyses confirmed that the enthalpy gains in the Chol-bristle driven multibilayer structure are much larger than that in the PC-bristle driven OPC structure. Another interesting finding was that in PGA-$Chol_{75}PC_{25}$ and PGA-$Chol_{50}PC_{50}$ the PC-bristles could promote to properly mobilize the overall brush polymer chains in the self-assembling process, thereby leading to the multibilayer structure formation with larger enthalpy gain.

Because of such the self-assembled nanostructure formations, PGA-$Chol_mPC_n$ polymers and their homopolymers always provided the film surface enriched with Chol and/or PC moieties which are mimicking biological cell membrane surface. The presences of PC- and Chol-bristles at the film surfaces were confirmed by XPS analysis. Higher Chol-enriched film surface showed lower water affinity, whereas higher PC-enriched film surface exhibited higher water affinity.

Overall, we have developed novel PGA-$Chol_mPC_n$ polymers, as a new cell membrane mimicking material system, which can favorably self-assemble multibilayer structure and provide biomolecular Chol- and PC-enriched surface. The PGA-$Chol_mPC_n$ polymers are very suitable for uses in the fields required cell membrane surface characteristics.

ASSOCIATED CONTENT

Supporting Information

The Supporting Information is available free of charge on the ACS Publications website at DOI: 10.1021/acs.macromol.7b00805.

NMR, IR, GPC, GIXS, and XPS data and GIXS data analysis (PDF)

AUTHOR INFORMATION

Corresponding Authors

*E-mail hskim@dongguk.ac.kr, Tel +82-54-770-2417, Fax +82-54-770-2447 (H.K.).

*E-mail ree@postech.edu, Tel +82-54-279-2120, Fax +82-54-279-3399 (M.R.).

ORCID

Moonhor Ree: 0000-0001-5562-2913

Author Contributions

C.K. and K.K. equally contributed to this work.

Notes

The authors declare no competing financial interest.

ACKNOWLEDGMENTS

This study was supported by the National Research Foundation of Korea (Haeksim Program 2015R1A2A2A2A01005642). The synchrotron X-ray scattering measurements at the Pohang Accelerator Laboratory were supported by MSIT, POSTECH Foundation, and POSCO Company.

REFERENCES

(1) Alberts, B.; Johnson, A.; Lewis, J.; Raff, M.; Roberts, K.; Walter, P. *Molecular Biology of the Cell*, 6th ed.; Garland Science: New York, 2014.

(2) Gennis, R. B. *Biomembranes − Molecular Structure and Function*; Springer-Verlag: New York, 1989.

(3) Krause, M. R.; Regen, S. L. The Structural Role of Cholesterol in Cell Membranes: From Condensed Bilayers to Lipid Rafts. *Acc. Chem. Res.* **2014**, *47*, 3512−3521.

(4) Goluszko, P.; Nowicki, B. Membrane Cholesterol: a Crucial Molecule Affecting Interactions of Microbial Pathogens with Mammalian Cells. *Infect. Immun.* **2005**, *73*, 7791−7796.

(5) Neef, A. B.; Schultz, C. Selective Fluorescence Labeling of Lipids in Living Cells. *Angew. Chem., Int. Ed.* **2009**, *48*, 1498−1500.

(6) Ikonen, S.; Macíčková-Cahová, H.; Pohl, R.; Šanda, M.; Hocek, M. Synthesis of Nucleoside and Nucleotide Conjugates of Bile Acids, and Polymerase Construction of Bile Acid-Functionalized DNA. *Org. Biomol. Chem.* **2010**, *8*, 1194−1201.

(7) Li, W.; Li, X.; Zhu, W.; Li, C.; Xu, D.; Ju, Y.; Li, G. Topochemical Approach to Efficiently Produce Main-Chain Poly(bile acid)s with High Molecular Weights. *Chem. Commun.* **2011**, *47*, 7728−7730.

(8) Nakaya, T.; Li, Y. J. Phospholipid Polymers. *Prog. Polym. Sci.* **1999**, *24*, 143−181.

(9) Yaseen, M.; Wang, Y.; Su, T. J.; Lu, J. R. Surface Adsorption of Zwitterionic Surfactants: n-Alkyl Phosphocholines Characterised by Surface Tensiometry and Neutron Reflection. *J. Colloid Interface Sci.* **2005**, *288*, 361−370.

(10) Pepys, M. B.; Hirschfield, G. M.; Tennent, G. A.; Gallimore, J. R.; Kahan, M. C.; Bellotti, V.; Hawkins, P. N.; Myers, R. M.; Smith, M. D.; Polara, A.; Cobb, A. J. A.; Ley, S. V.; Aquilina, J. A.; Robinson, C. V.; Sharif, I.; Gray, G. A.; Sabin, C. A.; Jenvey, M. C.; Kolstoe, S. E.; Thompson, D.; Wood, S. P. Targeting C-Reactive Protein for the Treatment of Cardiovascular Disease. *Nature* **2006**, *440*, 1217−1221.

(11) Milne, S. B.; Tallman, K. A.; Serwa, R.; Rouzer, C. A.; Armstrong, M. D.; Marnett, L. J.; Lukehart, C. M.; Porter, N. A.; Brown, H. A. Capture and Release of Alkyne-Derivatized Glycerophospholipids Using Cobalt Chemistry. *Nat. Chem. Biol.* **2010**, *6*, 205−207.

(12) Yu, X.; Liu, Z.; Janzen, J.; Chafeeva, I.; Horte, S.; Chen, W.; Kainthan, R. K.; Kizhakkedathu, J. N.; Brooks, D. E. Polyvalent Choline Phosphate as a Universal Biomembrane Adhesive. *Nat. Mater.* **2012**, *11*, 468−476.

DOI: 10.1021/acs.macromol.7b00805
Macromolecules 2017, 50, 6489−6500

(13) Jung, J. H.; Lim, Y. G.; Lee, K. H.; Koo, B. T. Synthesis of Glycidyl Triazolyl Polymers Using Click Chemistry. *Tetrahedron Lett.* **2007**, *48*, 6442−6448.
(14) Liu, D.; Zheng, Y.; Steffen, W.; Wagner, M.; Butt, H. J.; Ikeda, T. Glycidyl 4-Functionalized-1,2,3-Triazole Polymers. *Macromol. Chem. Phys.* **2013**, *214*, 56−61.
(15) Song, S.; Ko, Y.-G.; Lee, H.; Wi, D.; Ree, B. J.; Li, Y.; Michinobu, T.; Ree, M. High Performance Triazole-Containing Brush Polymers via Azide-Alkyne Click Chemistry: A New Functional Polymer Platform for Electrical Memory Devices. *NPG Asia Mater.* **2015**, *7*, e228−e240.
(16) Lee, B.; Park, Y.-H.; Hwang, Y.-T.; Oh, W.; Yoon, J.; Ree, M. Ultralow-*k* Nanoporous Organosilicate Dielectric Films Imprinted with Dendritic Spheres. *Nat. Mater.* **2005**, *4*, 147−150.
(17) Ree, M. Probing the Self-Assembled Nanostructures of Functional Polymers with Synchrotron Grazing Incidence X-Ray Scattering. *Macromol. Rapid Commun.* **2014**, *35*, 930−959.
(18) Kim, Y. Y.; Ree, B. J.; Kido, M.; Ko, Y.-G.; Ishige, R.; Hirai, T.; Wi, D.; Kim, J.; Kim, W. J.; Takahara, A.; Ree, M. High Performance n-Type Electrical Memory and Morphology-Induced Memory-Mode Tuning of A Well-Defined Brush Polymer Bearing Perylene Diimide Moieties. *Adv. Electronic Mater.* **2015**, *1*, 1500197.

DOI: 10.1021/acs.macromol.7b00805
Macromolecules 2017, 50, 6489−6500